Available online at www.sciencedirect.com
SCIENCE DIRECT®
Computers and Electronics in Agriculture 49 (2005) 255–271
Computers and electronics in agriculture
www.elsevier.com/locate/compag

Systemically diseased chicken identification using multispectral images and region of interest analysis☆

Chun-Chieh Yang[a], Kuanglin Chao[b,*], Yud-Ren Chen[b], Howard L. Early[c]

[a] *Department of Biosystems and Agricultural Engineering, University of Kentucky, Lexington, KY, USA*
[b] *Instrumentation and Sensing Laboratory, Agricultural Research Service, USDA, Beltsville, MD, USA*
[c] *Food Safety and Inspection Service, USDA, Washington, DC, USA*

Received 6 December 2004; received in revised form 18 April 2005; accepted 6 May 2005

Abstract

A simple image differentiation method for the identification of systemically diseased chickens was developed and cross-system validated using two different multispectral imaging systems. The first system acquired images at three wavelengths, 460 nm, 540 nm, and 700 nm, for a batch of 164 wholesome and 176 systemically diseased chicken carcasses. The second system acquired images at four wavelengths, 488 nm, 540 nm, 580 nm, and 610 nm, for a second batch of 332 wholesome and 318 systemically diseased chicken carcasses. Image masking was performed using the wavelengths of 700 nm and 610 nm for the first and second imaging systems, respectively. The relative reflectance intensity at individual wavelengths, ratio of intensities between pairs of wavelengths, and intensity combinations based on principal component analysis (PCA) were analyzed. It was found that the wavelengths of 540 nm and 580 nm are vital for successful chicken image differentiation. With proper wavelength selection, PCA can be useful for multispectral image analysis. The wavelength of 540 nm, selected as the key wavelength, was used in both imaging systems for image differentiation. An image processing algorithm was developed to define and locate the region of interest (ROI) as the differentiation area on the image. Based on ROI analysis, a single threshold was generated for image differentiation. The average relative reflectance intensity of the ROI was calculated for each chicken

☆ Mention of trade names or commercial products is solely for the purpose of providing specific information and does not imply endorsement or recommendation by the USDA.

* Corresponding author.
E-mail address: chaok@ba.ars.usda.gov (K. Chao).

0168-1699/$ – see front matter. Published by Elsevier B.V.
doi:10.1016/j.compag.2005.05.002

image. The classification and regression trees (CART) decision tree algorithm was used to determine the threshold value to differentiate systemically diseased chickens from wholesome ones. The first differentiation threshold, based on the first image batch and generated by the decision tree method, was applied to the second image batch for cross-system validation, and vice versa. The accuracy from validation was 95.7% for wholesome and 97.7% of systemically diseased chickens for the first image batch, and 99.7% for wholesome and 93.5% for systemically diseased chickens for the second image batch. The threshold values, each generated using only one of the two image batches, were similar. The results showed that using a single key wavelength and a threshold, this simple image processing and differentiation method could be used in automated on-line applications for chicken inspection. Published by Elsevier B.V.

Keywords: Food safety; Image analysis; Multispectral imagery; Poultry; Septicemia

1. Introduction

While seeking to improve the food safety inspection process to minimize food safety hazards, poultry plants must still continue to meet government food safety regulations, satisfy consumer demand, and maintain their competitiveness. The need for new inspection technologies (USDA, 1985), such as automated computer imaging inspection systems, has been recognized. Multispectral imaging is a non-destructive method and can obtain high classification accuracies for chicken conditions. It has great potential for use in high-speed on-line processing plant operations. Several studies have investigated the development of automated poultry inspection techniques based on multispectral imaging. Chao et al. (2002) developed a multispectral imaging system using the 540 nm and 700 nm wavelengths and obtained classification accuracies of 94% for wholesome and 87% for unwholesome chicken carcasses. Through hyperspectral imaging, Park et al. (2002) achieved from 97.3% to 100% accuracy in identifying fecal contamination and spilled tract material on poultry carcasses using images at the 434 nm, 517 nm, 565 nm, and 628 nm wavelengths. According to these studies, multispectral images contain spectral and spatial information from the surface of chicken carcass, which is essential for efficient identification of contaminated and systemically diseased chickens.

To achieve high classification accuracy, careful selection of key wavelengths is essential. Much research using visible/near infrared spectroscopy analysis has shown that certain wavelengths are particularly useful for the identification of diseased, contaminated, or defective chicken carcasses (Chao et al., 2003; Windham et al., 2003; Chen and Massie, 1993). Filters corresponding to those key wavelengths are then implemented for acquisition of multispectral images. After image acquisition, image processing algorithms are developed to adjust and analyze the images. With appropriate algorithms, specific features can be extracted from multispectral images to more suitably represent the classification target and increase the classification accuracy.

In considering practical on-line operations, the development of high accuracy multispectral image processing and differentiation algorithms that may be transferred to or implemented on different imaging systems would be very useful. Cross-system validation is important to evaluate an algorithm's practicability. Therefore, the main objective

of this study was to develop a simple multispectral image processing method that can be used for different imaging systems for differentiation of wholesome and systemically diseased chickens. Two multispectral imaging systems were built independently to collect images of wholesome and systemically diseased chickens. The image analyses were applied to select the key wavelength for differentiation purposes. The differentiation thresholds generated by images collected using each imaging system were then applied to differentiate among images collected by the other imaging system for cross-system validation.

2. Materials and methods

2.1. Sample collection

Eviscerated chicken carcasses were identified and collected by USDA FSIS veterinarians from a processing line at Allen Family Foods (Cordova, MD, USA). A total of 990 chicken carcasses were collected in two batches over a period from 2003 to 2004, of which 496 were wholesome carcasses and 494 were systemically diseased. The first batch of 164 wholesome and 176 systemically diseased chickens was collected and imaged between April and August of 2003. The second batch of 332 wholesome and 318 systemically diseased chickens was collected and imaged between November 2003 and April 2004. Systemically diseased chickens showed external symptoms of septicemia or toxemia. Septicemia is caused by the presence of pathogenic microorganisms or their toxins in the bloodstream, and toxemia is the result of toxins produced from cells at a localized infection or from the growth of microorganisms.

Chicken carcasses were collected from the processing line, placed in plastic bags, stored in coolers, and covered with ice to minimize dehydration. Then, the bags were transported to the Instrumentation and Sensing Laboratory (ISL) located in Beltsville, MD, USA within 2 h for imaging.

2.2. System development and image collection for the first imaging system

The first multispectral imaging system consisted of a common aperture camera (MS2100, DuncanTech, Auburn, CA, USA), a frame grabber (PCI-1428, National Instruments, Austin, TX, USA), an industrial computer (BSI, City of Industry, CA, USA), and eight 100 W tungsten halogen lights. The common aperture camera utilizes a color-separating prism to split broadband light entering the camera through the lens into three optical channels, and an interference filter and charge-coupled-device (CCD) imaging array are placed at each of the three exit planes of the prism to acquire separate images. In this study, the three optical channels were fitted with 460 nm (full width at half maximum, or FWHM, of 20.78 nm), 540 nm (18.31 nm FWHM) and 700 nm (17.40 nm FWHM) filters. It was found that a single waveband filter at a waveband longer than 600 nm can be used for image-masking (to select a threshold to separate the object and background); for this system, the 700 nm wavelength image was used for this purpose. Yang et al. (2005) describe details of the wavelength selection. The CameraLink utility program (DuncanTech, Auburn, CA, USA) was used to

control camera settings, such as triggering mode, output bit depth (eight bits), integration time of exposure, and analog gain. The frame grabber digitized the analog signals from the CCD imaging arrays. An eight-bit monochrome image was saved from each of the three channels.

The horizontal distance between the camera lens and the shackle to hold the chicken in the field of view was 813 mm. For each channel, the image size was 656 pixels × 493 pixels. The field of view was 397 mm × 298 mm; therefore, the image resolution was 0.37 mm^2 per pixel. Viewed from the shackle position, the eight tungsten halogen lights were arranged in four pairs, with two adjacent pairs 318 mm above the camera and two adjacent pairs 318 mm below the camera. Side by side, the two upper pairs spanned 190 mm, as did the two lower pairs. Viewed from the side, the upper pairs were positioned 267 mm from the field of view (546 mm from the camera) while the lower pairs were positioned slightly further at 305 mm from the field of view (508 mm from the camera). This lighting arrangement provided more illumination to the thigh and lower abdomen part of the chicken carcass, compensating for what would otherwise be insufficient lighting in this image area.

A spectralon diffuse reflectance target was used as a calibration target to determine the proper imaging integration time and gain for the lighting arrangement described above. The gain and integration times for spectralon imaging were set at 2 dB and 4.5 ms for the 700 nm channel, at 3 dB and 5.0 ms for the 540 nm channel, and at 9 dB and 9.5 ms for the 460 nm channel for calculating relative reflectance and for calibrating the chicken images. Chicken imaging used the same gain values but required longer integration times since the chicken reflectance was much lower than that of the spectralon. Accordingly, the integration time was set at 5 ms, 10 ms, and 18 ms for the 700 nm, 540 nm, and 460 nm channels, respectively. The same spectralon target was used to acquire calibration reference images prior to collection of chicken images; for acquiring the dark reference image, the camera lens was covered. For each chicken image, the chicken was hung on the shackle against a black background so that the chicken image could be easily extracted from the background.

2.3. System development and image collection for the second imaging system

The second multispectral imaging system used in this study consisted of a MultiSpec Imager™ spectrometer (Optical Insights, LLC, Santa Fe, NM, USA), a SpectraVideo™ SV 512 back-illuminated CCD camera (PixelVision Inc., Tigard, OR, USA), a PMB-004 shutter and cooler control board, a PMB-007 serial interface board, a PMJ-002 PCI bus data acquisition board, a LynxPCI™ frame grabber, a Pentium-III 600 PC computer (Gateway, Poway, CA, USA), and four 100 W tungsten halogen lights. Four interference filters and an optical mirror assembly were used to create four waveband images of the target that were acquired simultaneously on a single CCD focal plane. The resulting 16-bit multispectral image contained four sub-images. The PixelView version 3.20 utility program (PixelVision Inc., Tigard, OR, USA) was used to control camera settings, such as integration time and image acquisition. The filter parameters selected for this system were 10 nm FWHM at 488 nm, 10 nm FWHM at 540 nm, 10 nm FWHM at 580 nm, and 10 nm FWHM at 610 nm. The 610 nm wavelength image was used for image masking; Yang et al. (2004) describe details of wavelength selection.

The distance between the camera lens and the chicken sample field of view was 1143 mm. Four tungsten halogen lights were mounted 610 mm from the field of view, on a rectangular frame. During image collection, the spectralon diffuse reflectance target was used as a calibration target for flat field correction. Because the part of the carcass that required more illumination when using the first imaging system was excluded by a smaller field of view when using this second imaging system, it was unnecessary to compensate for insufficient lighting in this case.

Unlike the first imaging system, the second imaging system simultaneously acquired four sub-images (one for each waveband) on a single CCD focal plane. Consequently, appropriate selection of a single integration time resulting in a clear image safely below saturation levels at all wavebands was essential. Through trial-and-error, it was found that using an integration time of 500 ms, along with a (pre-set) high gain setting, was long enough to reduce noise in the short-wavelength sub-images (460 nm and 540 nm) and short enough to avoid over-saturation in the long-wavelength sub-images (580 nm and 610 nm) and in flat field calibration. These settings were used for both flat field calibration and acquisition of the chicken images. The cooling temperature for the camera control unit was set at 251 K.

Because each image in the second image batch consisted of sub-images on the single CCD focal plane, the image registration process was required to precisely locate each sub-image. The 460 nm sub-image was located at the upper left quadrant, the 540 nm sub-image at the upper right quadrant, the 580 nm sub-image at the lower right quadrant, and the 610 nm sub-image at the lower left quadrant of the original image. The pixel x–y-coordinates were defined with (0, 0) in the upper leftmost corner of the original image. A grid paper with four pre-defined points was used for image registration. In an image of the grid paper, each sub-image showed each of the four points as a single pixel. The 610 nm sub-image in the lower left quadrant, a 214 pixels $\times$ 241 pixels area defined by four boundary points at (282, 20), (282, 260), (495, 260), and (495, 20), was used as the base image in determining the offset vectors between the 610 nm sub-image and the other three sub-images. The offset vectors were used to determine the boundaries of the other three sub-images corresponding to the boundaries of the 610 nm sub-image. The resolution of all the sub-images was 0.87 mm^2 per pixel.

Again, each chicken was hung on the shackle for imaging against a black background so that the chicken image could be easily extracted from the background. Furthermore, for both imaging systems, the same spectralon reference target was used to acquire the calibration reference images prior to collection of chicken images, and the dark reference image was acquired with the camera lens covered. This step is essential for applying the same image differentiation method to different imaging systems. Because the relative reflectance images of chicken carcasses were always taken based on the white reference image of the same spectralon reference target and the dark reference image of the covered lens, the images from two different imaging systems could be used for the same differentiation method.

2.4. Multispectral image processing and region of interest (ROI) identification

After collecting images from both imaging systems, image processing steps were performed, using MATLAB 6.1 (MathWorks Inc., Natick, MA, USA), to obtain single-channel images for image analysis, as diagrammed in Fig. 1 for the first image batch and Fig. 2 for

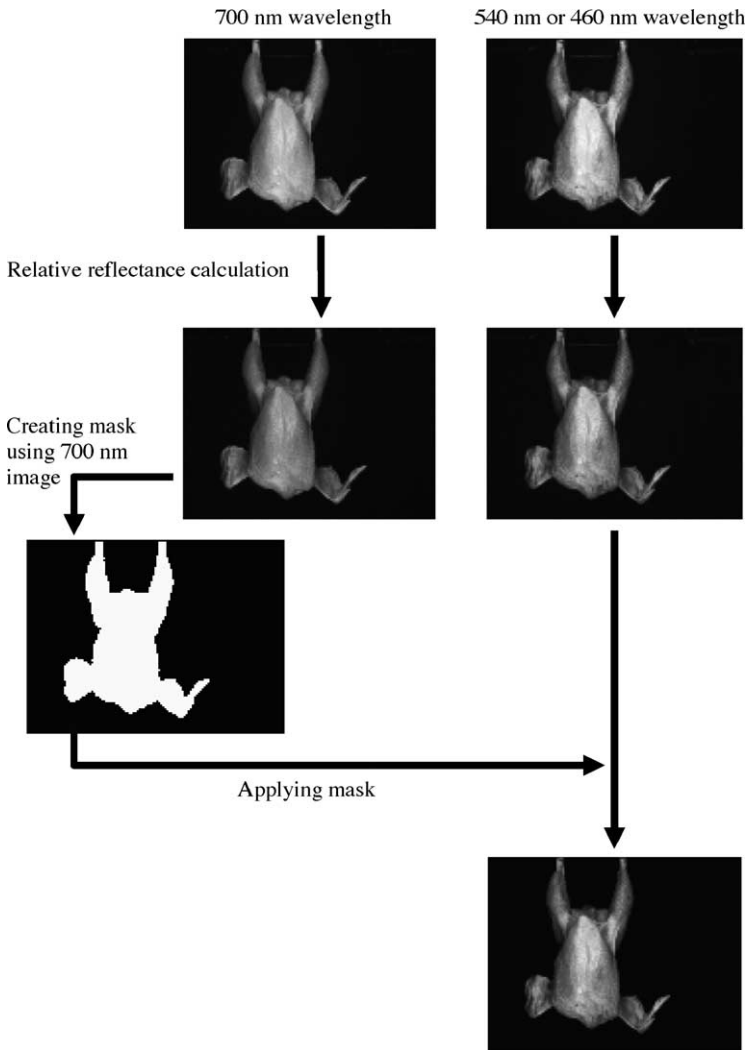

Fig. 1. Image processing for the first imaging system.

the second image batch. First, flat field correction, the essential step for cross-system image differentiation, was performed according to the equation,

$$I = \frac{I_0 - B}{W - B} \tag{1}$$

where I_0 is the original image, B the dark reference image, W the white spectralon reference image, and I is the relative reflectance image. Second, the 700 nm image in the first batch and the 610 nm sub-image in the second batch were used to build image masks. It was observed that for both batches, the relative intensity for the black background was always

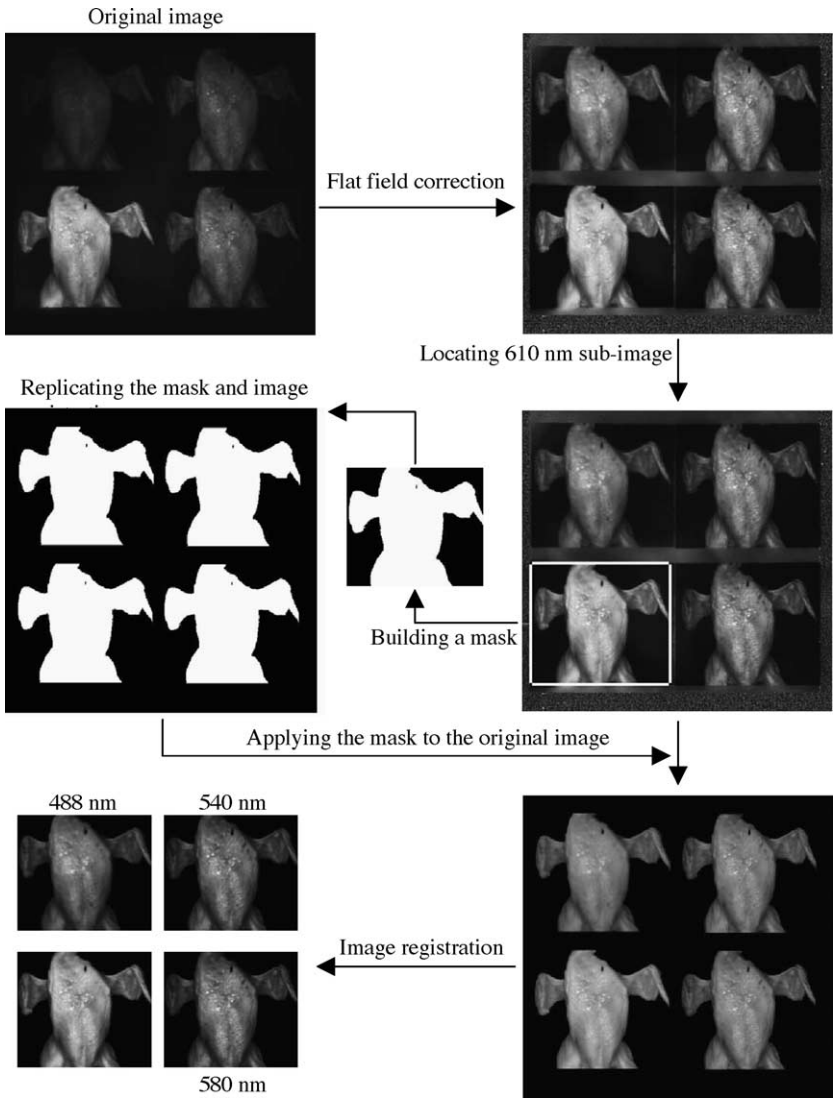

Fig. 2. Image processing, to obtain single-channel sub-images for the second imaging system.

<0.1 and the chicken intensity was always >0.1. Thus, the threshold value of 0.1 was used to create the mask. Third, for each batch, the mask was applied to the other wavelength images to remove the background. This resulted in the background pixels of each image being reset to zero; for other pixels, the intensity values remained the same. Then, for only the second image batch, the other three wavelength sub-images were then separated from the original images using the vectors of image registration.

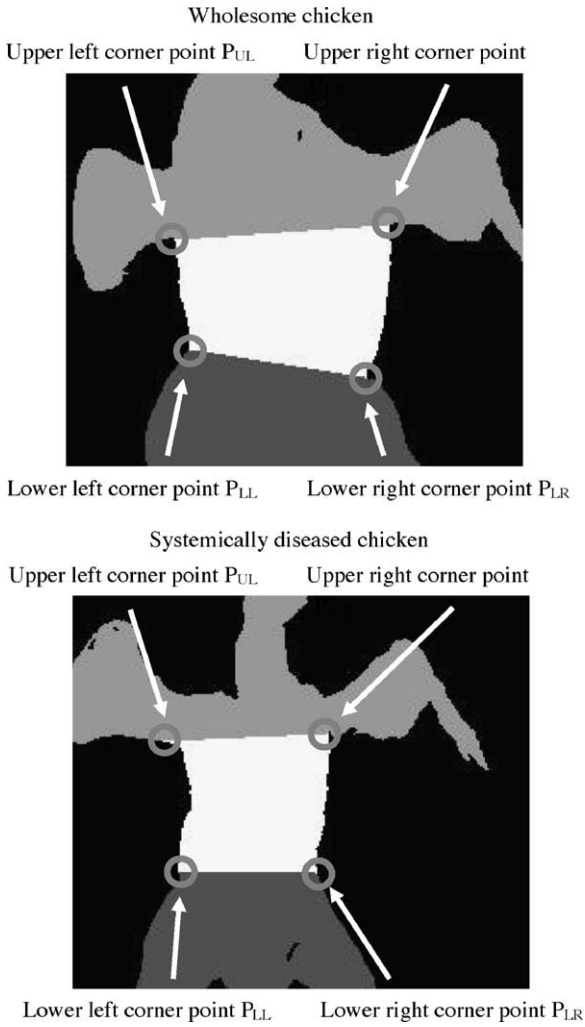

Fig. 3. Definition of region of interest (ROI) areas by four corner points.

It has been observed that the major differences between wholesome and systemically diseased chicken occur between the breast and lower abdomen (Yang et al., 2004). Therefore, for proper differentiation of systemically diseased chickens from wholesome chickens, the region of interest was defined around this area. To find the ROI boundaries on an image, four corner points must be located as shown in Fig. 3. The lower left and lower right corner points were the conjunction points between abdomen and thigh along the chicken boundary. The upper left and upper right corner points were the conjunction points between abdomen and wing along the chicken boundary. Using the mask image, the boundary of the chicken carcass was identified. Fig. 4 illustrates the search operation for the lower left and upper right ROI corner points. As shown in Fig. 4, the lowest point of the boundary, which was on the

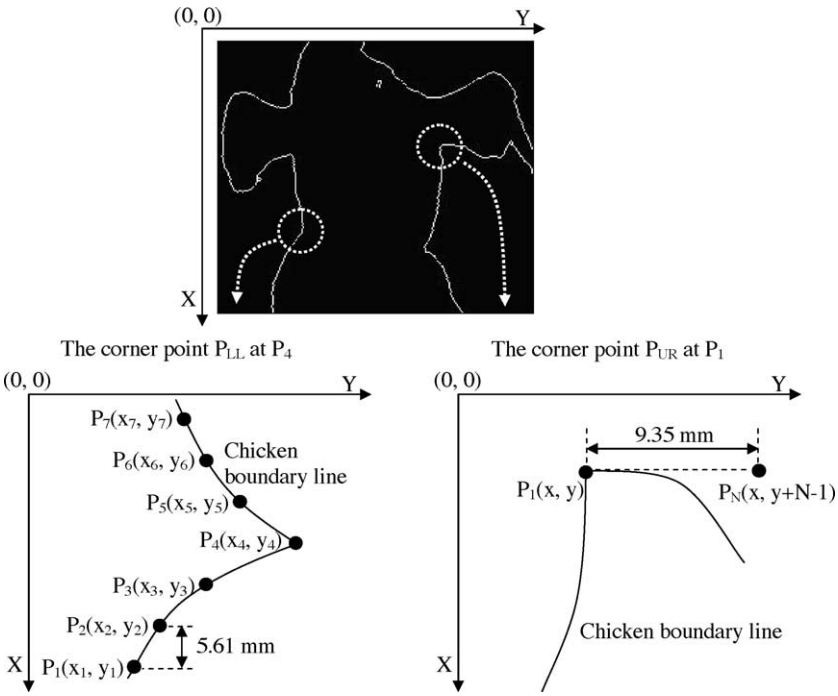

Fig. 4. Search operation for the ROI corner points.

thigh, was then located as the start point P_1. From this start point along the boundary, seven points were located, noted as $P_1(x_1, y_1)$ to $P_7(x_7, y_7)$, the distance d where $d = x_i - x_{i-1}$ was approximately 5.61 mm, nine pixels in the first batch, and six pixels in the second batch. Based on trial-and-error, it was found that the corner point would be missed if the distance d were shorter or longer than 5.61 mm and the boundary was not a smooth curve or, in some cases, not a continuous line. The following relational and logical operations were carried out:

$$A_L = \{(y_{j+1} - y_j \geq 0) \text{ and } (y_{j+2} - y_{j+1} \geq 0) \text{ and } (y_{j+3} - y_{j+2} \geq 0)\} \quad (2)$$

$$B_L = \{(y_{j+3} - y_{j+4} \geq 0) \text{ and } (y_{j+4} - y_{j+5} \geq 0) \text{ and } (y_{j+5} - y_{j+6} \geq 0)\} \quad (3)$$

$$C_L = \{(y_{j+3} - y_{j+4} \leq 0) \text{ and } (y_{j+4} - y_{j+5} \leq 0) \text{ and } (y_{j+5} - y_{j+6} \leq 0)\} \quad (4)$$

$$D_L = \{(y_{j+3} - y_{j+4} < y_{j+4} - y_{j+5}) \text{ and } (y_{j+4} - y_{j+5} < y_{j+5} - y_{j+6})\} \quad (5)$$

$$T_L = \{(A_L) \text{ and } ((B_L) \text{ or } ((C_L) \text{ and } (D_L)))\} \quad (6)$$

When the logical value of T_L was false, the point at the boundary line and adjacent to the start point P_1 was selected as the new start point, and thus, another seven points were located to repeat the operations. Empirically, at the first instance at which the logical value of T_L was true, the point P_4 was at the conjunction point between chicken thigh and abdomen,

and thus, this point was defined as the lower left corner point P_{LL}. Similarly, the following relational and logical operations were carried out to determine the lower right corner point:

$$A_R = \{(y_{j+1} - y_j \leq 0) \text{ and } (y_{j+2} - y_{j+1} \leq 0) \text{ and } (y_{j+3} - y_{j+2} \leq 0)\} \quad (7)$$

$$B_R = \{(y_{j+3} - y_{j+4} \leq 0) \text{ and } (y_{j+4} - y_{j+5} \leq 0) \text{ and } (y_{j+5} - y_{j+6} \leq 0)\} \quad (8)$$

$$C_R = \{(y_{j+3} - y_{j+4} \geq 0) \text{ and } (y_{j+4} - y_{j+5} \geq 0) \text{ and } (y_{j+5} - y_{j+6} \geq 0)\} \quad (9)$$

$$D_R = \{(y_{j+3} - y_{j+4} > y_{j+4} - y_{j+5}) \text{ and } (y_{j+4} - y_{j+5} > y_{j+5} - y_{j+6})\} \quad (10)$$

$$T_R = \{(A_R) \text{ and } ((B_R) \text{ or } ((C_R) \text{ and } (D_R)))\} \quad (11)$$

The operations were repeated until the first instance at which the logical value of T_R was true, upon which the point P_4 was defined as the lower right corner point P_{LR}.

From the lower left corner point $P_{LL}(x_i, y_j)$, the point $P_1(x_i - i, y_k)$ in the boundary line was located, and N pixels from $P_1(x_i - i, y_k)$ to $P_N(x_i - i, y_k - (N-1))$ were compared to the chicken boundary. The distance between P_1 and P_N was approximately 9.35 mm; thus, the number N was 15 for the first batch and 10 for the second batch. Along the chicken boundary, this operation would be repeated until all pixels from P_1 to P_N were all within the chicken boundary, which indicated the starting point of the chicken wing. Therefore, the point P_1 would be defined as the upper left corner point P_{UL}. Similarly, from the lower right corner point $P_{LR}(x_i, y_j)$, the point $P_1(x_i - 1, y_k)$ in the boundary line was located, and N pixels from $P_1(x_i - 1, y_k)$ to $P_N(x_i - 1, y_k + (N-1))$ were compared to the chicken boundary. This operation was repeated along the chicken boundary, so that the point P_1 was determined as the upper right corner point P_{UR}.

After the four corner points were located, the straight line between P_{LL} and P_{LR}, the straight line between P_{UL} and P_{UR}, the segments of the chicken boundary lines between P_{LL} and P_{UL} and between P_{LR} and P_{UR} were defined as the ROI boundary.

2.5. Image differentiation

To investigate a proper differentiation method, three image features were calculated: average relative reflectance intensity, average ratio of relative reflectance intensity, and average principal component value. First, the average relative reflectance intensity from ROI at each single wavelength was calculated for each relative reflectance image. The average intensities at 460 nm and 540 nm wavelengths (AI_{460} and AI_{540}) were obtained for each image of the first image batch. The average intensities at 488 nm, 540 nm, and 580 nm wavelengths (AI_{488}, AI_{540}, and AI_{580}) were obtained for each image of the second image batch.

Second, the average of the ratio of relative reflectance intensity from ROI between two wavelengths was calculated for each image. Thus, the average intensity ratio between 540 nm and 460 nm wavelengths ($AR_{540/460}$) was obtained for the first image batch. Three average intensity ratios between 540 nm and 488 nm wavelengths ($AR_{540/488}$), between 580 nm and 488 nm wavelengths ($AR_{580/488}$), and between 580 nm and 540 nm wavelengths ($AR_{580/540}$) were obtained for the second image batch.

Third, the average intensity of principal component from ROI was calculated for each image. This feature was calculated using the covariance eigenvectors generated by principal component analysis (PCA). PCA calculates the eigenvectors of the covariance matrix and approximates the original data by a linear combination of the leading eigenvectors. For a multispectral image of k spectral wavelengths, each with $m \times n$ pixels, the image data is reorganized into two-dimensional array X of size s by k where $s = m \times n$. The covariance matrix of X is defined as:

$$C_x = \frac{\overline{X}^{\mathrm{T}}\overline{X}}{s-1} \tag{12}$$

where C_x is a matrix of size $k \times k$, and $\overline{X}$ is the $s \times k$ mean-centered matrix of X, determined by first calculating the mean for each column, and then subtracting the column mean from each value in that column. In the PCA decomposition, the p_i vectors are eigenvectors of the covariance matrix C_x. For each p_i:

$$C_x p_i = \lambda_i p_i \tag{13}$$

where λ_i is the eigenvalue associated with the covariance eigenvector p_i. Each principal component PC_i is denoted by:

$$\mathrm{PC}_i = \sum_{j=1}^{k} \overline{X}_j p_{ji} \tag{14}$$

Each principal component is a weighted sum of the reflectance intensity from k wavelengths.

In this study, multispectral images of 10 wholesome and 10 systemically diseased sample chickens collected from the same time period as the first image batch, and of another 10 wholesome and 10 systemically diseased sample chickens from the same time period as the second image batch, were used for PCA calculation. Each of the sample images was mean centered, i.e. for each wavelength, the average intensity from the image was subtracted from the relative reflectance intensity of each pixel. Singular value decomposition was performed using MATLAB-based PLS Toolbox 3.0 (Eigenvector Research Inc., Manson, WA, USA) to calculate the eigenvectors p_i of the covariance matrix C_x for each of the 20 sample chickens. The average covariance eigenvector p_i values were calculated for the sample chickens.

After obtaining the average intensities and covariance eigenvectors of the sample chickens for each image batch, the images at each batch were mean centered, and then, the principal components were calculated for each chicken. The average intensity of principal component images (APC) was then calculated for analysis.

The classification and regression trees (CART) decision tree algorithm (Breiman et al., 1984) was used to generate a threshold to differentiate wholesome and systemically diseased chickens, using the AnswerTree 3.0 program (SPSS, Chicago, IL). CART was selected because this algorithm has been applied successfully to many differentiation and classification applications (Balk and Elder, 2000; Eisenberg and McKone, 1998; Pietersma et al., 2003; Yang et al., 2005). The details of CART processing could be referred to Breiman et al. (1984). In order to obtain a single threshold for simple differentiation, the maximum tree level (i.e. the maximum number of splits) was set at one to obtain the threshold. The cross-system validation of image differentiation is the primary object of this study; therefore,

to evaluate the performance of the differentiation method, two tests were carried out based on the decision tree method. For first test, the threshold was generated using the first image batch and then applied to differentiating the images in the second batch. For the second test, the threshold generated using the second image batch was applied to differentiating the first image batch.

3. Results and discussion

3.1. Principal component analysis

Table 1 lists the results of PCA for 20 sample chickens for the first image batch and another 20 sample chickens for the second image batch. For the 10 wholesome and 10 systemically diseased sample chickens collected at the same time period as the first image batch, the standard deviation for the average covariance eigenvector is only 0.0321 for $\overline{X}_{540}$ and 0.0599 for $\overline{X}_{460}$. The first principal component captured 83.41% of the total variance in the 20 sample images. These results show that the first principal component image could adequately represent the total variance of the original image. Therefore, the covariance eigenvectors in Table 1 were used to determine the weighted sum value of the first principal component PC_1 for each image from the first image batch according to the equations below:

$$PC_1 = \overline{X}_{540} \times 0.6543 + \overline{X}_{460} \times 0.5543 \quad (15)$$

where $\overline{X}_{540}$ and $\overline{X}_{460}$ are the mean-centered relative reflectance intensities at the 540 nm and 460 nm wavelengths, respectively. The average intensity of the first principal component image for each image was then calculated for image differentiation.

For the 10 wholesome and 10 systemically diseased sample chickens collected at the same time period as the second image batch, the standard deviation for the average covariance eigenvector is also small: 0.0328 for $\overline{X}_{488}$, 0.0158 for $\overline{X}_{540}$, and 0.0186 for $\overline{X}_{580}$. The first principal component captured 99.63% of the total variance in the 20 sample images. The results also indicate that the first principal component image could adequately represent the total variance of the original image. Therefore, the covariance eigenvectors in Table 1 were used to determine the weighted sum value of the first principal component PC_1 for each image from the second image batch according to the equation below:

$$PC_1 = \overline{X}_{488} \times 0.5836 + \overline{X}_{540} \times 0.5552 + \overline{X}_{580} \times 0.5912 \quad (16)$$

Table 1
Principal component analysis (PCA) results at the first principal component (PC_1) for sample chickens

	Wavelength, X (nm)	Eigenvector, p	Standard deviation for eigenvector, p
First image batch	540	0.6543	0.0321
	460	0.5543	0.0599
Second image batch	488	0.5836	0.0328
	540	0.5552	0.0158
	580	0.5912	0.0186

where $\overline{X}_{488}$, $\overline{X}_{540}$, and $\overline{X}_{580}$ are the mean-centered relative reflectance intensities at the 488 nm, 540 nm, and 480 nm wavelengths, respectively. The average intensity of the first principal component image for each image was then calculated for image differentiation.

3.2. Image differentiation

Table 2 lists the results for image differentiation using a single threshold generated by the decision tree method using AI, AR, and APC, respectively. The results show that PCA could be applied to multispectral image analysis for accurate differentiation. For the first image batch, the differentiation accuracies using APC were 100% for wholesome chickens and 94.32% for systemically diseased chickens. For the second image batch, the differentiation accuracies using APC were 90.66% for wholesome chickens and 92.77% for systemically diseased chickens. The accuracy for APC was slightly lower than those using AI_{540} and AI_{580} but much higher than those using AR. The high differentiation accuracies using APC show that the intensity of the first principal component image can be used for multispectral image differentiation between wholesome and systemically diseased chickens. With proper wavelength selection, principal component analysis would be applied to multispectral images in order to obtain a simple intensity combination from multispectral wavelengths.

From Table 2, AI_{540} and AI_{580} could be used for proper differentiation since the differentiation accuracies using the average intensity from each of the 540 nm and 580 nm wavelengths were high. The accuracies for image differentiation using AI_{540} and AI_{580} in the second image batch were all higher than 96% for wholesome chickens and 99% for systemically diseased chickens. Liu and Chen (2001) found that the reflectance from these two wavelengths closely relates to symptoms manifesting from the relative oxymyoglobin levels found in systemically diseased chickens. The result clearly shows that the 540 nm and 580 nm wavelengths are very useful for differentiation.

Table 2
Image differentiation accuracies using a single threshold generated by decision tree

		Wholesome (%)	Systemically diseased (%)	Threshold
First image batch	AI_{540}	100.0	97.16	0.2572
	AI_{460}	96.34	90.34	0.2093
	$AR_{540/460}$	49.36	73.86	1.1760
	APC	100.0	94.32	0.2567
Second image batch	AI_{488}	92.77	83.65	0.2710
	AI_{540}	96.39	100.0	0.2626
	AI_{580}	96.69	99.69	0.3009
	$AR_{540/488}$	92.17	50.00	0.8992
	$AR_{580/488}$	93.37	50.63	0.9511
	$AR_{580/540}$	80.72	57.86	1.0586
	APC	90.66	92.77	−0.0647

First image batch: 164 wholesome chickens and 176 systemically diseased chickens; second image batch: 332 wholesome chickens and 318 systemically diseased chickens; AI_i: the average intensity at *i* nm wavelength; $AR_{i/j}$: the average intensity ratio between *i* nm and *j* nm wavelengths; APC: the average principal component combination value.

The differentiation accuracies using the average intensities from the 460 nm and 488 nm wavelengths were relatively low for systemically diseased chickens, at 90.34% for AI_{460} for the first image batch, and at 83.65% for AI_{488} for the second image batch. The result shows that the 460 nm and 488 nm wavelengths may contain insufficient information for differentiation, compared to the 540 nm and the 580 nm wavelengths. Unlike the 540 nm and 580 nm wavelengths, the 460 nm and 488 nm wavelengths cannot be used alone for differentiation. This situation may also cause the poor differentiation using $AR_{540/460}$, $AR_{540/488}$, and $AR_{580/488}$, as shown by the low differentiation accuracies in Table 2.

Although the accuracies for AI_{540} and AI_{580} were high, which indicated that these two wavelengths contain useful and essential information for differentiation, the average intensity ratio between these two wavelengths, $AR_{580/540}$, was still too poor to be used for differentiation. The reason for this conflict situation could be that the low reflectance intensities of the 540 nm and the 580 nm wavelengths are indicative of the same oxymyoglobin-related symptom of systemically diseased chickens (Liu and Chen, 2001). Because of this and examining the image detail, it is found that the relative magnitude of the average intensity for the same chicken compared to other chickens would be the same between the 540 nm and 580 nm wavelengths. Mathematically, the average intensity ratio between these two wavelengths would be close to a constant. Therefore, $AR_{580/540}$ cannot be used for differentiation.

From Table 2, it is evident that differentiation was more successful using the average intensity (AI) at a single wavelength or the average intensity of the first principal component image of multispectral images. Because only the 540 nm wavelength was used in both imaging systems, only the average intensity from this wavelength (AI_{540}) was used for further cross-system validation.

3.3. Cross-system validation for image differentiation

Table 3 shows the differentiation accuracies for different tests. For the first test, the differentiation accuracies for the first image batch were 100% for wholesome chickens and 97.2% for systemically diseased chickens. The generated threshold, 0.2572, was then applied to the second image batch and resulted in differentiation accuracies of 99.7% for wholesome chickens and 93.5% for systemically diseased chickens. For the second test, the decision tree classified the second image batch with accuracies of 96.4% for wholesome

Table 3
Image differentiation accuracies for cross-imaging validation of imaging systems

		First image batch (%)	Second image batch (%)
First test	Wholesome	100	99.7
	Systemically diseased	97.2	93.5
	Threshold	0.2572	0.2572
Second test	Wholesome	95.7	96.4
	Systemically diseased	97.7	100
	Threshold	0.2626	0.2626

First image batch: 164 wholesome chickens and 176 systemically diseased chickens and second image batch: 332 wholesome chickens and 318 systemically diseased chickens.

chickens and 100% for systemically diseased chickens. The generated threshold, 0.2626, then correctly classified 95.7% of wholesome chickens and 97.7% of systemically diseased chickens for the first image batch.

The results clearly showed that using a single threshold generated by the CART decision tree method could perform an accurate differentiation between wholesome and systemically diseased chickens when using the average relative reflectance intensity from the ROI area at the single waveband of 540 nm as an input. The average intensity at 540 nm from wholesome chicken is consistently higher than the average intensity from systemically diseased chicken; therefore, the waveband at 540 nm can reflect differences between wholesome and systemically diseased chicken condition (Liu and Chen, 2001). Moreover, the threshold values changed by only 2.06% from one imaging system to another. The high accuracy of the differentiation rate and consistent threshold value evidently indicated that this simple method could be used in different imaging systems, which is important for real-world applications.

The results also showed that differentiation performed better for systemically diseased chickens when a larger sample population (the second image batch) was used for determining the threshold value. The differentiation rate for systemically diseased chickens increased by 4.2% from the first test (335 training images) to the second test (638 training images); however, the differentiation rate decreased by 4.0% for wholesome chickens. Assuming that public concern would value increased assurance of food safety over economic benefit, the threshold generated at the second test, 0.2626, might be more appropriate for application.

Using the average relative reflectance intensity from the ROI area is helpful for differentiation because the areas excluded by ROI, such as the wings and thighs, would contribute a number of pixels where the difference of intensity between wholesome and systemically diseased chickens was less significant to the average intensity calculation. This phenomenon can be observed more clearly from the contour images in Fig. 5. From the contour images, it is evident that the major intensity differences between wholesome and systemically diseased chickens occur between the breast and lower abdomen. The intensity difference for breast and thighs is less significant, and the intensity difference for wings is hardly observed. Also, illumination factors affecting chicken sample presentation could make the ROI area feasible for inspection based on image analysis methods. In presenting a chicken carcass for image acquisition, providing uniform illumination across the entire chicken carcass is a great challenge. Spectral features from the chicken breast area are least affected by physical shape. Shadows will always occur on peripheral areas of the carcass, such as the wings, thighs, and sides of the chicken.

A single waveband filter at 540 nm and one additional filter at a waveband longer than 600 nm for image-masking purposes (such as 610 nm or 700 nm) could be implemented for identification of systemically diseased chickens by an automated on-line multispectral imaging system using a simple average relative reflectance intensity calculation. The ROI area defined in this study is best suited for the sample handling and presentation requirements of an automated on-line spectral imaging system. The algorithm proposed in this study to identify the ROI area can be applied to images from different imaging systems even when the resolutions and the fields of view in these systems are different from each other. The result of the cross-system validation in this study can be considered satisfactory.

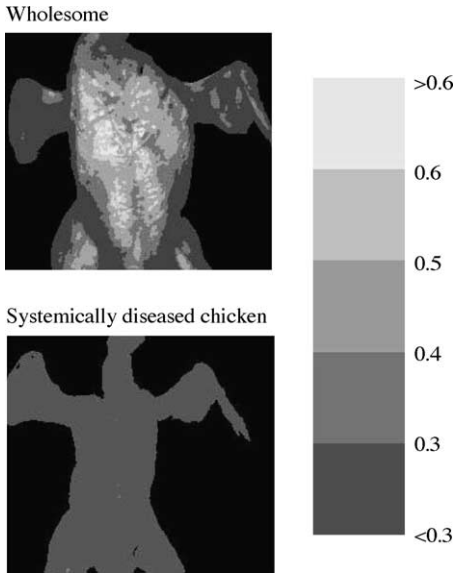

Fig. 5. Contour images at the 540 nm wavelength for wholesome and systemically diseased chickens.

4. Conclusions

In this study, a simple multispectral image processing and differentiation method was developed to differentiate wholesome and systemically diseased chickens in different imaging systems. It was found that the wavelengths of 540 nm and 580 nm are the key wavelengths for differentiation between wholesome and systemically diseased chickens. It was also found that principal component analysis could be applied to multispectral images for spectral combination without losing essential information at each wavelength for accurate differentiation. Because of significant color differences that occur between wholesome and systemically diseased chickens at 540 nm, an interference filter at that wavelength was selected for implementation as the key wavelength for two different multispectral imaging systems. An algorithm was developed to find the ROI on the multispectral images from different imaging systems with different resolutions and the fields of view. Prior to collection of chicken images, it was essential that the same spectralon white reference target was used for both imaging systems to acquire calibration reference images and that the camera lens was covered on both imaging systems to acquire the dark reference image. This step was to allow the differentiation method developed based on one system could be applied to the other system. This transferability is very useful for real-world application. With the average relative reflectance intensity as the input, differentiation thresholds for identifying wholesome and systemically diseased chickens were determined using the CART decision tree algorithm.

Using the differentiation threshold generated from the first image batch (0.2572), differentiation accuracies for wholesome and systemically diseased chickens were 100% and 97.2%, respectively, for the first image batch, and were 99.7% and 93.5%, respectively,

for the second image batch. Using the differentiation threshold generated from the second image batch (0.2626), differentiation accuracies for wholesome and systemically diseased chickens were 96.4% and 100%, respectively, for the second image batch, and were 95.7% and 97.7%, respectively, for the first image batch. This differentiation method, using the simple calculation of average relative reflectance intensity, showed significant potential for testing in an automated on-line multispectral imaging inspection system.

References

Balk, B., Elder, K., 2000. Combining binary decision tree and geostatistical methods to estimate snow distribution in a mountain watershed. Water Resour. Res. 36, 13–26.

Breiman, L., Friedman, J.H., Olshen, R.A., Stone, C.J., 1984. Classification and Regression Trees. Wadsworth, Belmont, CA.

Chao, K., Chen, Y.R., Hruschka, W.R., Gwozdz, F.B., 2002. On-line inspection of poultry carcasses by a dual-camera system. J. Food Eng. 51, 185–192.

Chao, K., Chen, Y.R., Chan, D.E., 2003. Analysis of vis/NIR spectral variations of wholesome, septicemia, and cadaver chicken carcasses. Appl. Eng. Agric. 19, 453–458.

Chen, Y.R., Massie, D.R., 1993. Visible/near-infrared reflectance and interactance spectroscopy for detection of abnormal poultry carcasses. Trans. ASAE 36, 863–869.

Eisenberg, J.N.S., McKone, T.E., 1998. Decision tree method for the classification of chemical pollutants: incorporation of across-chemical variability and within-chemical uncertainty. Environ. Sci. Technol. 32, 3396–3404.

Liu, Y., Chen, Y.R., 2001. Analysis of visible reflectance spectra of stored, cooked and diseased chicken meats. Meat Sci. 58, 395–401.

Park, B., Lawrence, K.C., Windham, W.R., Buhr, R.J., 2002. Hyperspectral imaging for detecting fecal and ingesta contamination on poultry carcasses. Trans. ASAE 45, 2017–2026.

Pietersma, D., Lacroix, R., Lefebvre, D., Wade, K.M., 2003. Performance analysis for machine-learning experiments using small data sets. Comput. Electron. Agric. 38, 1–17.

USDA, 1985. Meat and Poultry Inspection. Committee on the Scientific Basis of the Nation's Meat and Poultry Inspection Program. National Academy Press, Washington, DC.

Windham, W.R., Smith, D.P., Park, B., Lawrence, K.C., Feldner, P.W., 2003. Algorithm development with visible/near-infrared spectra for detection of poultry feces and ingesta. Trans. ASAE 46, 1733–1738.

Yang, C.-C., Chao, K., Chen, Y.R., Kim, M.S., 2004. Application of multispectral imaging for identification of systemically diseased chicken. ASAE Paper No. 043034, Am. Soc. Agric. Eng., St. Joseph, MI.

Yang, C.-C., Chao, K., Chen, Y.R., 2005. Development of multispectral imaging processing algorithms for identification of wholesome, septicemia, and inflammatory process chickens. J. Food Eng. 69, 225–234.